

Article

# Insights over Titanium Modified FeMgO<sub>x</sub> Catalysts for Selective Catalytic Reduction of NO<sub>x</sub> with NH<sub>3</sub>: Influence of Precursors and Crystalline Structures

Liting Xu <sup>1</sup>, Qilei Yang <sup>2</sup>, Lihua Hu <sup>1</sup>, Dong Wang <sup>2,\*</sup>, Yue Peng <sup>2</sup>, Zheru Shao <sup>1</sup>, Chunmei Lu <sup>3</sup> and Junhua Li <sup>2</sup>

<sup>1</sup> Everbright Environmental Protection Technological Development (Nanjing) Limited, Nanjing 210000, China; xuliting@ebchinaintl.com.cn (L.X.); hulh@ebchinaintl.com.cn (L.H.); shaozr@ebchinaintl.com.cn (Z.S.)

<sup>2</sup> State Key Joint Laboratory of Environment Simulation and Pollution Control, National Engineering Laboratory for Multi Flue Gas Pollution Control Technology and Equipment, School of Environment, Tsinghua University, Beijing 100084, China; yangqilei@tsinghua.edu.cn (Q.Y.); pengyue83@tsinghua.edu.cn (Y.P.); lijunhua@tsinghua.edu.cn (J.L.)

<sup>3</sup> School of Energy and Power Engineering, Shandong University, Jinan 250061, China; cml@sdu.edu.cn

\* Correspondence: sdu\_wd@tsinghua.edu.cn; Tel.: +86-010-6278-2030

Received: 3 May 2019; Accepted: 17 June 2019; Published: 24 June 2019



**Abstract:** Titanium modified FeMgO<sub>x</sub> catalysts with different precursors were prepared by coprecipitation method with microwave thermal treatment. The iron precursor is a key factor affecting the surface active component. The catalyst using FeSO<sub>4</sub> and Mg(NO<sub>3</sub>)<sub>2</sub> as precursors exhibited enhanced catalytic activity from 225 to 400 °C, with a maximum NO<sub>x</sub> conversion of 100%. Iron oxides existed as γ-Fe<sub>2</sub>O<sub>3</sub> in this catalyst. They exhibited highly enriched surface active oxygen and surface acidity, which were favorable for low-temperature selective catalytic reduction (SCR) reaction. Besides, it showed advantage in surface area, spherical particle distribution and pores connectivity. Amorphous iron-magnesium-titanium mixed oxides were the main phase of the catalysts using Fe(NO<sub>3</sub>)<sub>3</sub> as a precursor. This catalyst exhibited a narrow T<sub>90</sub> of 200/250–350 °C. Side reactions occurred after 300 °C producing NO<sub>x</sub>, which reduced the NO<sub>x</sub> conversion. The strong acid sites inhibited the side reactions, and thus improved the catalytic performance above 300 °C. The weak acid sites appeared below 200 °C, and had a great impact on the low-temperature catalytic performance. Nevertheless, amorphous iron-magnesium-titanium mixed oxides blocked the absorption and activation between NH<sub>3</sub> and the surface strong acid sites, which was strengthened on the γ-Fe<sub>2</sub>O<sub>3</sub> surface.

**Keywords:** selective catalytic reduction (SCR); catalyst; precursor; NO<sub>x</sub> conversion

## 1. Introduction

Nitrogen oxides (NO<sub>x</sub>) mainly come from fossil fuel combustion [1–3] and have caused a series of environmental problems such as nitric acid rain, photochemical smog, ozone layer depletion and fine particle pollution [4–7]. As the severe NO<sub>x</sub> emission situation and the rigorous emission legislation exhibit, many efforts have been made in NO<sub>x</sub> reduction [8]. SCR (selective catalytic reduction) of NO<sub>x</sub> with NH<sub>3</sub> [9–12] has been extensively proved to be the most efficient way for the removal of NO<sub>x</sub> from stationary sources. A catalyst is critical to create an efficient SCR reaction and operating cost [13]. Commercial catalysts, such as V<sub>2</sub>O<sub>5</sub>/TiO<sub>2</sub>, V<sub>2</sub>O<sub>5</sub>-WO<sub>3</sub>/TiO<sub>2</sub> and V<sub>2</sub>O<sub>5</sub>-MoO<sub>3</sub>/TiO<sub>2</sub> [8,14–18], were constrained for further development because of several inevitable drawbacks such as high cost, the bio-toxicity of the common vanadium compounds, etc. [19,20]. Furthermore, the commercial

vanadium-titanium catalysts have been managed as hazardous waste. The study of novel high-efficiency catalysts is of great significance.

Many efforts have been made on iron oxides based catalysts, such as Fe-Ti [21–23], Fe/Ce-Ti [24,25], Fe-Ce-W [26,27], Fe-Sn-Mn [28], Ce-Fe/WMH [29],  $\text{WO}_3/\text{Fe}_2\text{O}_3$  [30], Fe/ $\text{WO}_3\text{-ZrO}_2$  [31], Mn-Fe/ $\text{TiO}_2$  [32],  $\text{FeMnTiO}_x$  [33], etc. Iron oxides catalysts have low prices and free secondary pollution. They showed good catalytic performance and high  $\text{N}_2$  selectivity for SCR reaction [8,34,35].  $\text{NO}_x$  conversion of 60% was obtained over  $\text{Fe}_2\text{O}_3/\text{TiO}_2$  prepared by Kato in 250–450 °C. In Fe/ $\text{WO}_3\text{-ZrO}_2$  [31], Fe-Mn-Ce/ $\gamma\text{-Al}_2\text{O}_3$  [36], and Fe-Er-V/ $\text{TiO}_2\text{-WO}_3\text{-SiO}_2$  [37], the introduce of iron enlarged the surface area and pore volume, and meanwhile, it improved the Brønsted and Lewis acid sites. Zhu [38] studied Co-Fe/ $\text{TiO}_2$  and Cu-Fe/ $\text{TiO}_2$  and manifested that the reactants could be easily adsorbed on Co-Fe/ $\text{TiO}_2$  because of its strong adsorption capacity, while Cu-Fe/ $\text{TiO}_2$  showed better redox ability. The redox ability and surface acidity are the key factors that affect the catalytic performance. As far as we know, the type of precursors is the very first factor that could have great impact on the physicochemical properties of catalysts. It plays a decisive role on the surface active component, the surface area, the redox ability, the surface acidity, etc. Liu [39,40] et al prepared  $\text{FeTiO}_x$  via coprecipitation with  $\text{Fe}(\text{NO}_3)_3$  and  $\text{Ti}(\text{SO}_4)_2$  as precursors. The catalyst exhibited good  $\text{NH}_3\text{-SCR}$  activities and the  $\text{NO}_x$  conversion exceeded 90% in 200–350 °C. They found that there was strong interaction between iron and titanium. Ma [41] prepared  $\text{Fe}_2(\text{SO}_4)_3/\text{TiO}_2$  by the impregnation method and found the  $\text{NO}_x$  conversion was up to 98% in 350–450 °C. Heterogeneous agglomeration of iron oxides could be weakened and the Brønsted acid sites could be improved by using  $\text{Fe}_2(\text{SO}_4)_3$  as a precursor. In our previous work [42–44], we found that the magnesium-based catalyst showed good SCR activity and sulfur tolerance. Furthermore we studied on titanium modified  $\text{FeMgO}_x$  catalysts and found that titanium modified  $\text{FeMgO}_x$  catalysts exhibited excellent catalytic performance in SCR reaction. However, to the best of our knowledge, the catalytic performance could be further improvement via modifying the precursors.

In this work, a series of titanium modified  $\text{FeMgO}_x$  catalysts with different precursors were studied. The objective of this paper is to investigate the effect of precursor type on the physicochemical properties of titanium modified  $\text{FeMgO}_x$  catalysts and to reveal the optimization mechanism of catalytic performance.

## 2. Experimental

### 2.1. Catalyst Preparation

$\text{FeSO}_4\cdot 7\text{H}_2\text{O}$ ,  $\text{FeCl}_2\cdot 7\text{H}_2\text{O}$  and  $\text{Fe}(\text{NO}_3)_3\cdot 9\text{H}_2\text{O}$  were used as iron precursors,  $\text{Mg}(\text{NO}_3)_2\cdot 6\text{H}_2\text{O}$  and  $\text{MgSO}_4\cdot 7\text{H}_2\text{O}$  (analytical pure, Tianjin Kermel Chemical Reagent Co., Ltd, Tianjin, China) were used as magnesium precursors and  $\text{NH}_3\cdot \text{H}_2\text{O}$  was used as precipitant in catalyst preparation. Titanium modified  $\text{FeMgO}_x$  catalysts were prepared via coprecipitation method with microwave thermal treatment. A certain amount of iron precursor, magnesium precursor and  $\text{TiSO}_4$  (analytical pure, Sinopharm Group Co., Ltd, Shanghai, China) were dissolved in 250 mL deionized water and sufficiently stirred for 1 h.  $\text{NH}_3\cdot \text{H}_2\text{O}$  was titrated into the mixed solution with continuous stirring until the pH of the mixed solution was 9–10. Then the precipitate was filtered and washed by deionized water several times until neutral to remove the foreign ions. The precipitate was first impregnated by 1 mol/L  $\text{Na}_2\text{CO}_3$  solution and then disposed of by microwave thermal treatment. The impregnated precipitate was washed by deionized water to be neutral and then dried at 105 °C. After calcined at 400 °C for 5 h, the obtained sample was crushed and sieved into 40–60 mesh (0.28 nm–0.45 nm) for the test. The catalysts prepared were denoted as Ti modified  $\text{FeMgO}_x$  with label SN, SS, CN, CS, NN and NS to represent different combination of precursors (S represents for sulfates, N represents for nitrates and C represents for chlorides), as seen in Table 1.

**Table 1.** Titanium modified FeMgO<sub>x</sub> catalysts with different precursors.

Label	Catalyst	Precursor
SN	Ti modified FeMgO <sub>x</sub>	FeSO <sub>4</sub> ·7H <sub>2</sub> O, Mg(NO <sub>3</sub> ) <sub>2</sub> ·6H <sub>2</sub> O
SS		FeSO <sub>4</sub> ·7H <sub>2</sub> O, MgSO <sub>4</sub> ·7H <sub>2</sub> O
CN		FeCl <sub>2</sub> ·7H <sub>2</sub> O, Mg(NO <sub>3</sub> ) <sub>2</sub> ·6H <sub>2</sub> O
CS		FeCl <sub>2</sub> ·7H <sub>2</sub> O, MgSO <sub>4</sub> ·7H <sub>2</sub> O
NN		Fe(NO <sub>3</sub> ) <sub>3</sub> ·9H <sub>2</sub> O, Mg(NO <sub>3</sub> ) <sub>2</sub> ·6H <sub>2</sub> O
NS		Fe(NO <sub>3</sub> ) <sub>3</sub> ·9H <sub>2</sub> O, MgSO <sub>4</sub> ·7H <sub>2</sub> O

## 2.2. Activity Test

NH<sub>3</sub>-SCR activity was completed in a quartz fixed-bed tube reactor at atmosphere pressure. The simulated flue gas was provided with standard gases, including 0.1 Vol % NO, 0.1 Vol % NH<sub>3</sub>, 3.5 Vol % O<sub>2</sub> and balanced N<sub>2</sub>. The total flow rate of simulated gas was 2 L/min and the catalyst used in each experiment was 4 mL, thus the corresponding gas hourly space velocity (GHSV) was 30,000/h<sup>-1</sup>. The concentration of NO and NO<sub>2</sub> was monitored and analyzed by the MGA5 Flue Gas Analyzer (MRU Instruments, Inc. Emission Monitoring Systems, Neckarsulm-Obereisesheim, Germany). Before entering the flue gas analyzer, the flue gas should be washed by phosphoric acid (100% pure) to absorb ammonia and avoid the impact of ammonia on the analyzer. Data were recorded every 25 °C from 100 °C to 400 °C. NO<sub>x</sub> conversion was calculated as follows:

$$\eta = \frac{C[\text{NO}_x(\text{inlet})] - C[\text{NO}_x(\text{outlet})]}{C[\text{NO}_x(\text{inlet})]} \times 100\% \quad (1)$$

where C[NO<sub>x</sub>(inlet)] and C[NO<sub>x</sub>(outlet)] meant the concentration of NO<sub>x</sub> in the inlet and outlet of the reactor, μL/L. NO<sub>x</sub> represented the sum of NO and NO<sub>2</sub>.

## 2.3. Catalyst Characterization

A Rigaku D/max 2500 PC diffractometer (50 kV × 150 mA) with Cu Kα radiation was used to complete the X-ray Diffraction. The data of 2θ were collected from 10° to 90° by 4 °/min with the step size 0.1°.

N<sub>2</sub>-adsorption-desorption was obtained by using an ASAP2020 Surface Area and Porosity Analyzer (Micromeritics Instrument Corp., Norcross, Georgia, USA) at −196 °C. The specific surface area and the average pore diameter were calculated by the Brunauer–Emmett–Teller (BET) method, and the specific pore volume and pore diameter distribution were calculated by Barrett–Joyner–Halenda (BJH) method.

Microstructure of the catalysts was conducted on a Japan JSM-6700F cold field emission scanning electron microscope. The elements on the surface of the catalysts were analyzed on an Oxford INCA X sight energy dispersive spectrometer (Be4-U92) with 5.9 KeV, UK.

To analyze the surface atomic concentration and distinguish the chemical states of the elements, a Thermo ESCALAB 250XI surface analyze system with Al Kα radiation (1486.6 eV, 150 W) was used to complete X-ray Photoelectron Spectroscopy. Prior to the measurement, each sample was degassed in vacuum to eliminate surface contamination.

Temperature-programmed Desorption of NH<sub>3</sub> (NH<sub>3</sub>-TPD) was performed on a TP-5080 instrument using a 100 mg sample. The sample was pretreated in flowing He at 300 °C for 1 h before the measurement. Then, the sample was He-cooled to 100 °C, then treated with 5% NH<sub>3</sub>/Ar at a flow rate of 30 mL/min for 0.5 h and flushed with He at 100 °C for 1 h. The desorption process was carried out by heating the sample from 100 °C to 700 °C at a rate of 10 °C/min.

### 3. Results and Discussion

#### 3.1. Effect of Different Precursors on Catalytic Performance Over Titanium Modified FeMgO<sub>x</sub> Catalysts

The catalytic performance of titanium modified FeMgO<sub>x</sub> catalysts with different precursors is shown in Figure 1. It was obvious that temperature had a strong effect on titanium modified FeMgO<sub>x</sub> catalysts with different precursors at the temperature range from 100 to 400 °C. Generally speaking, it was necessary to reach a certain temperature for the catalyst to exhibit good catalytic activity, while an excessively high reaction temperature would lead to a decrease in catalytic activity due to the secondary reaction.

Titanium modified FeMgO<sub>x</sub> catalysts with different precursors revealed excellent catalytic activity from 100 to 400 °C and had wide temperature windows. Among all the catalysts, catalysts SN, SS, CN and CS showed similar catalytic performances, which was distinctly evident with catalysts NN and NS. When the temperature was below 200 °C, catalyst NN and NS showed better catalytic activity than other catalysts, especially catalyst NN, whose NO<sub>x</sub> conversion could exceed 50% and 90% when the reaction temperature was close to 150 °C and 200 °C, respectively. However, when the temperature exceeded 350 °C, the NO<sub>x</sub> conversion of catalysts NN and NS apparently decreased to about 50–60% due to the oxidation and decomposition of NH<sub>3</sub>. The NO<sub>x</sub> conversion of catalysts SN, SS, CS and CN could be stable at 90% at high temperature range. Among all the catalysts, catalyst SN with precursors of FeSO<sub>4</sub> and Mg(NO<sub>3</sub>)<sub>2</sub> exhibited excellent catalytic activity and N<sub>2</sub> selectivity in a wide temperature range, with NO<sub>x</sub> conversion above 90% from 225 to 400 °C and N<sub>2</sub> selectivity above 90% in the whole temperature range. The NO<sub>x</sub> conversion of which approached 100% from 250 to 375 °C.

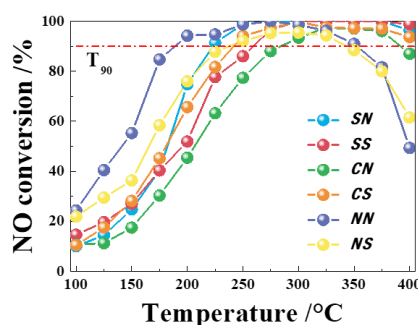


**Figure 1.** Catalytic performance of titanium modified FeMgO<sub>x</sub> catalysts with different precursors.

#### 3.2. X-ray Diffraction (XRD) Patterns

Figure 2 shows the XRD patterns of titanium modified FeMgO<sub>x</sub> catalysts with different precursors. There were no diffraction peaks of magnesium or titanium in XRD patterns of all the catalysts according to JCPDF standard; it could be inferred that magnesium and titanium existed in a highly dispersed state or an amorphous state in the catalyst, or maybe that the crystallites formed were less than 5 nm. There were obvious sharp diffraction peaks of the catalysts SN, SS, CN and CS at  $2\theta = 30.2^\circ$ ,  $35.5^\circ$ ,  $43.2^\circ$ ,  $53.7^\circ$ ,  $53.7^\circ$  and  $62.8^\circ$ , corresponding to maghemite ( $\gamma$ -Fe<sub>2</sub>O<sub>3</sub>) crystallite according to JCPDS PDF#39-1346 [39,40]. It could be inferred that maghemite crystallite was the main active component in these catalysts.

However, in catalyst NN and NS, the diffraction peaks were ascribed to amorphous oxides, comparing with that in Figure S1. It could be concluded that the active component was directly affected by the precursors. When Fe(NO<sub>3</sub>)<sub>3</sub> was used as precursor, the active components of the titanium modified FeMgO<sub>x</sub> catalysts prepared were iron-magnesium-titanium mixed oxides; however, when FeSO<sub>4</sub> and FeCl<sub>2</sub> were used as precursors, the active component of the titanium modified FeMgO<sub>x</sub> catalysts prepared was  $\gamma$ -Fe<sub>2</sub>O<sub>3</sub>. It was reported that  $\gamma$ -Fe<sub>2</sub>O<sub>3</sub> was an octahedral structure with vacancies and was in a metastable state with a lower activation energy, which resulted in better denitration activity. In general, different active components led to diversity between different catalysts.

Considering the result of the activity test, iron-magnesium-titanium mixed oxides and  $\gamma$ -Fe<sub>2</sub>O<sub>3</sub> as active components were the substantial cause of different catalytic performance. The mixed oxides made the temperature window of the catalysts NN and NS obviously shift to a low temperature range and was the main cause of the secondary reaction at high temperature range.

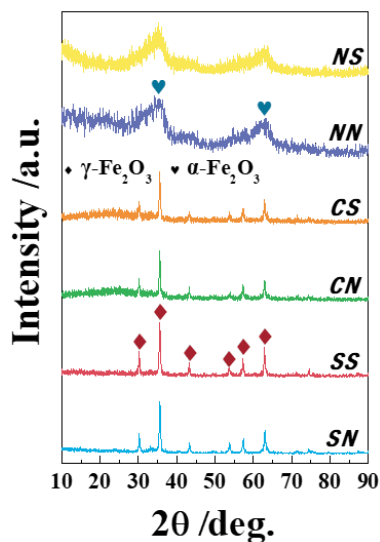


**Figure 2.** Powder X-ray diffraction (XRD) patterns of titanium modified FeMgO<sub>x</sub> catalysts with different precursors.

### 3.3. N<sub>2</sub>-Adsorption-Desorption

BET surface area, average pore volume and average pore diameter of titanium modified FeMgO<sub>x</sub> catalysts with different precursors are enumerated in Table 2.

**Table 2.** Surface characterization of titanium modified FeMgO<sub>x</sub> catalysts with different precursors.

Catalysts	S <sub>BET</sub> /m <sup>2</sup> ·g <sup>-1</sup>	V <sub>BJH</sub> /cm <sup>3</sup> ·g <sup>-1</sup>	Average Pore Diameter/nm
SN	55.1245	0.2291	16.2670
SS	46.6441	0.1951	18.6213
CN	58.6066	0.2413	15.5461
CS	51.8948	0.2243	19.2990
NN	181.3934	0.2279	4.3710
NS	180.4130	0.2340	4.4512

The BET surface area, BJH pore volume and average pore diameter of the catalysts SN, SS, CN and CS were similar to each other. The BET surface area of catalyst SN, which exhibited the best catalytic activity, was 55.1245 m<sup>2</sup>/g, the pore volume was 0.2291 cm<sup>3</sup>/g and the average pore diameter was 16.2670 nm. Nevertheless, the BET surface area of the catalysts NN and NS using Fe(NO<sub>3</sub>)<sub>3</sub> as a precursor were 181.3934 m<sup>2</sup>/g and 180.4130 m<sup>2</sup>/g, respectively, which were three times larger than the other four catalysts. The average pore diameter of the catalysts NN and NS were only 4.3710 nm and 4.4512 nm, which were almost four times smaller than the other four catalysts, but the pore volumes were close to each other. Generally speaking, more active sites could be provided by large surface area, pore volume and relatively small average pore diameter, which was beneficial for SCR reaction. For the catalysts NN and NS, large surface area could provide more active sites, but the small pore diameter would lead to the increment of diffusion resistance during the gas-solid reaction and would be bad for the adsorption-desorption process. Appropriate surface area, pore volume and average pore diameter in the catalyst SN could provide enough active sites and guarantee the diffusion and mass transfer processes, which were in favor of SCR reaction.

t-Plot microporous area and volume are enumerated in Table 3. It was obvious that the t-Plot microporous area was much smaller than t-Plot external surface area, and the microporous volume of all the catalysts was close to zero. It could be concluded that the t-Plot microporous area had less contribution to the surface area, and the t-Plot external surface area was much more important to produce large surface area. Meanwhile, mesopore (pore diameter ranging from 2 to 50 nm) was the main pore type in titanium modified FeMgO<sub>x</sub> catalysts with different precursors, and there were substantially fewer micropores (pore diameter less than 2 nm).

**Table 3.** t-Plot properties of titanium modified FeMgO<sub>x</sub> catalysts with different precursors.

Samples	t-Plot Microporous Area/m <sup>2</sup> ·g <sup>-1</sup>	t-Plot External Surface Area/m <sup>2</sup> ·g <sup>-1</sup>	t-Plot Microporous Volume/cm <sup>3</sup> ·g <sup>-1</sup>
SN	0.5467	54.5777	6.5000 × 10 <sup>-5</sup>
SS	5.1114	41.5327	2.5290 × 10 <sup>-3</sup>
CN	4.3249	54.2817	2.0670 × 10 <sup>-3</sup>
CS	6.5865	45.3083	3.3030 × 10 <sup>-3</sup>
NN	2.7968	178.5966	3.5550 × 10 <sup>-4</sup>
NS	3.1251	177.2879	2.54 × 10 <sup>-3</sup>

Distribution characterization of pore structures over titanium modified FeMgO<sub>x</sub> catalysts with different precursors is shown in Figure 3. In Figure 3a,b, pore diameter of all the catalysts is distributed mainly from 2 nm to 10 nm, which also means that mesopores were the major pore type in the catalysts. In addition, the pore diameter distribution of the catalysts NN and NS is obviously distinguished from the other catalysts, and the intensities of the distribution peaks are a great deal stronger than other catalysts, indicating that the pores ranging from 2 to 10 nm made a greater contribution to surface area and pore volume.

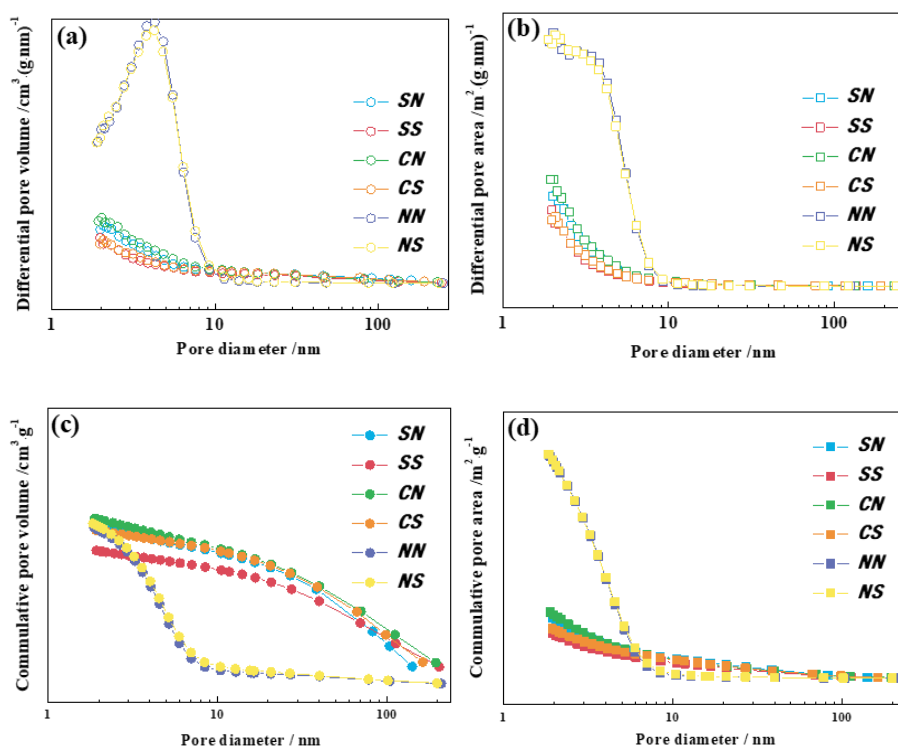


**Figure 3.** Distribution characterization of pore structures over titanium modified FeMgO<sub>x</sub> catalysts with different precursors: (a) Pore volume, (b) Pore area, (c) Cumulate pore volume and (d) Cumulate pore area.

In Figure 3c,d, it can be seen that the cumulative pore area and the cumulative pore volume of the catalysts SN, SS, CN and CS gently declined with pore diameter. However, the cumulative pore area and the cumulative pore volume of the catalysts NN and NS from 2 to 10 nm declined rapidly with pore diameter, and the cumulative pore area and the cumulative pore volume above 10 nm were pretty small compared with that from 2 to 10 nm. The intensive distribution of pore diameter from 2 to 10 nm could provide a large surface area, but the narrow distribution of pore diameter would lead to the hysteresis of the diffusion and mass transfer processes. For the catalyst SN, the reasonable distribution of pore diameter could guarantee enough surface area and also the diffusion and mass transfer processes.

The  $N_2$ -adsorption-desorption isotherms of titanium modified  $FeMgO_x$  catalysts are shown in Figure 4. According to the International Union of Pure and Applied Chemistry classification, the  $N_2$ -adsorption-desorption isotherms of the catalysts SN, SS, CN and CS were classified as V-shaped isotherms with an H3 hysteresis loop. The absorbed volume was really small when the pressure was low. Only when the pressure was approaching the saturated vapor pressure did the absorbed volume increase rapidly due to capillary condensation. The absorption characteristic was often observed by the weak solid-gas interaction in mesopores on the surface of catalysts. It could be concluded from the type of isotherm and hysteresis loop that disorderly wedge-shaped mesopores were formed by particles accumulated loosely on the surface of the catalysts [44].

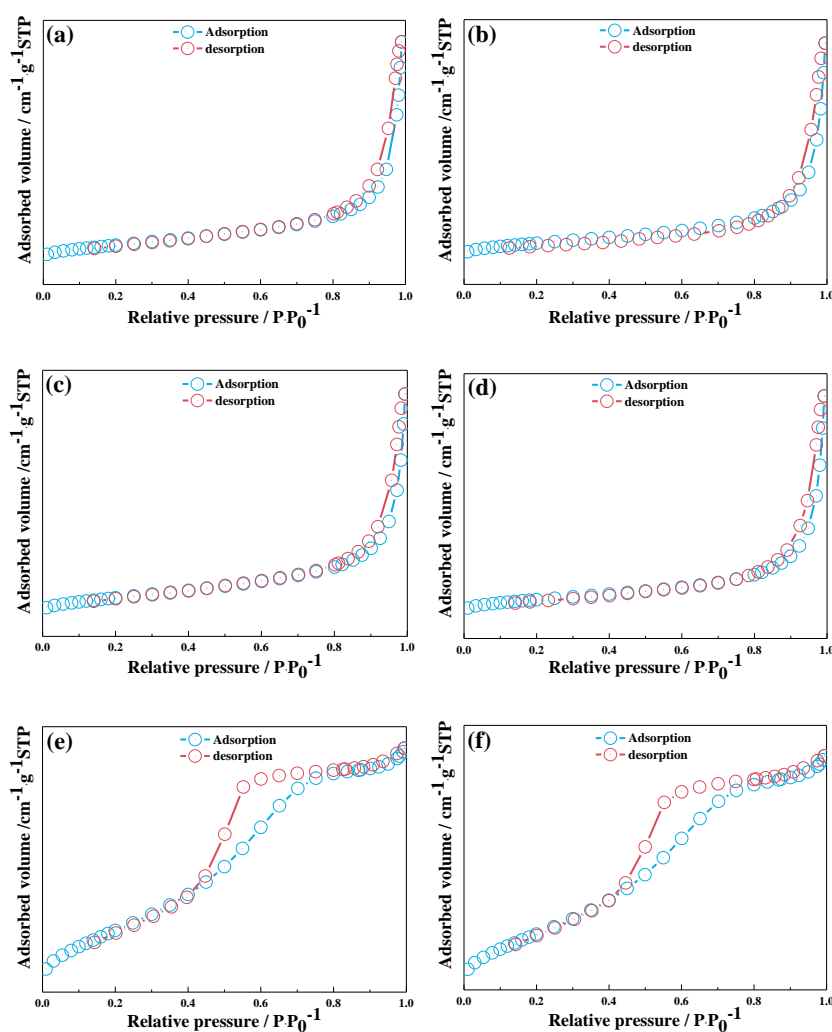


**Figure 4.**  $N_2$ -adsorption-desorption isotherms of titanium modified  $FeMgO_x$  catalysts with different precursors: (a) SN, (b) SS, (c) CN, (d) CS, (e) NN and (f) NS.

However, the  $N_2$ -adsorption-desorption isotherms of the catalysts NN and NS were classified as IV-shaped isotherms with an H4 hysteresis loop. The absorbed volume gradually increased when the pressure was low. Only when the relative pressure was about 0.5 to 0.8 did the absorbed volume increase rapidly, and then the absorbing capacity became almost invariable, which meant there were mainly mesopores in the catalysts and less macropores were obtained. It could be concluded from the type of isotherm and hysteresis loop that wedge-shaped mesopores were formed by lamellar structures accumulated tightly on the surface of the catalysts.

#### 3.4. SEM and Energy Dispersive Spectrometer (EDS)

The SEM images of titanium modified  $FeMgO_x$  catalysts are shown in Figure 5. The surface of the catalysts SN, SS, CN and CS presented spherical particle distribution and the particles were significantly more independent and regular. There was hardly any accumulation of particles occurring on the surface of these catalysts, and the regular distribution of particles benefitted the formation of intergranular pores, which were good for the mass transfer process.

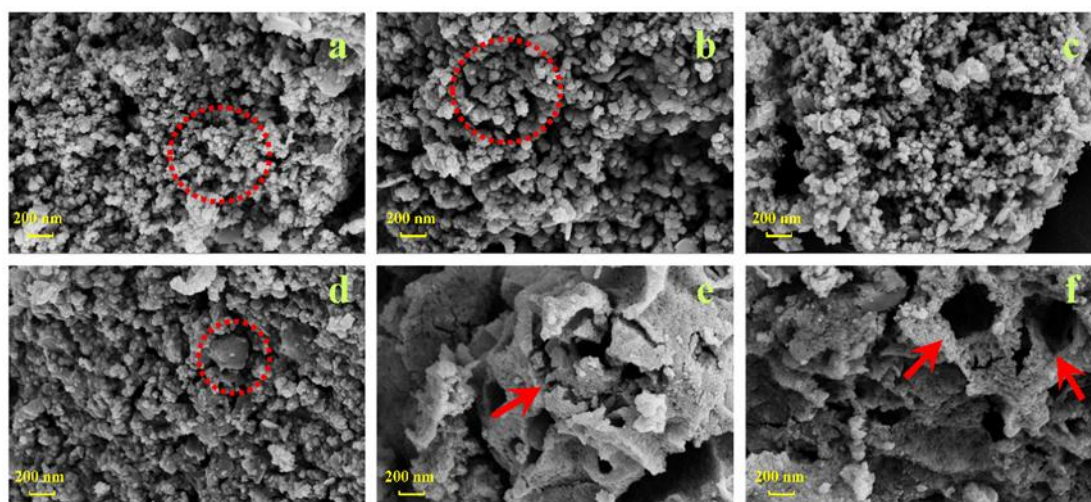


**Figure 5.** SEM images of titanium modified  $FeMgO_x$  catalysts with different precursors: (a) SN, (b) SS, (c) CN, (d) CS, (e) NN and (f) NS.

However, the surface of the catalysts NN and NS exhibited stratiform and nubby distribution. There were a huge number of pyknotic fine intergranular pores on the stratiform and nubby structure. Fine intergranular pores were favorable for large surface area and provided more active sites, but they would resist the diffusion and mass transfer process. Meanwhile the results implied that the choice of an iron precursor had significant influence on the surface morphology of the catalyst. The catalyst SN exhibited regular and distributed spherical particles with good pores connectivity which were favor of SCR reaction.

The EDS composition analysis of titanium modified  $FeMgO_x$  catalysts with different precursors is shown in Table 4.

**Table 4.** EDS composition analysis data of titanium modified FeMgO<sub>x</sub> catalysts with different precursors.

Catalyst	Percentage by Weight/wt %				Percentage by Atomicity/at %			
	Fe	Mg	Ti	O	Fe	Mg	Ti	O
SN	59.06	1.68	4.79	34.47	30.82	2.85	3.21	63.12
SS	59.25	3.10	4.73	32.92	31.72	3.81	2.95	61.52
CN	60.66	3.64	4.60	31.10	33.16	4.57	2.93	59.34
CS	59.33	3.18	4.40	33.09	31.68	3.90	2.74	61.68
NN	68.39	2.90	5.30	23.41	41.97	4.09	3.79	50.16
NS	67.93	3.47	4.88	23.72	41.53	4.45	3.17	50.85

The catalysts prepared all consisted of iron, magnesium, titanium and oxygen, as expected. From Table 4, it can be seen that the percentage of oxygen by atomicity of the catalysts NN and NS was obviously lower than that of the catalysts SN, SS, CN and CS, which means that it was difficult for oxygen atoms to enrich on the surface of the catalysts NN and NS. The percentage of oxygen by atomicity of the catalyst SN could reach 63.12%. In general, the surface oxidation ability could be improved by the abundant lattice oxygen on the surface of the catalyst. Strong oxidation ability could promote NO oxidation to NO<sub>2</sub> and then induce the rapid SCR reaction, which effectively guarantees the catalytic performance of the catalyst. The results illustrated that using Fe(NO<sub>3</sub>)<sub>3</sub> as a precursor was not conducive to the enrichment of oxygen on the surface of the catalyst.

### 3.5. X-ray Photoelectron Spectroscopy (XPS)

An XPS test was used to better elucidate the species, concentration and valency of different elements on the surface of titanium modified FeMgO<sub>x</sub> catalysts with different precursors, and the element surface concentration calculated is shown as Table 5. It can be seen that the main elements of titanium modified FeMgO<sub>x</sub> catalysts are iron, magnesium, titanium and oxygen, which is in agreement with EDS results.

**Table 5.** X-ray photoelectron spectroscopy (XPS) elementary surface concentration of titanium modified FeMgO<sub>x</sub> catalysts with different precursors.

Catalyst	Fe 2p/%	Mg 1s/%	O 1s/%	Ti 2p/%
SN	38.88	6.92	46.85	7.35
SS	46.35	7.89	37.20	8.57
CN	45.75	9.54	37.75	6.95
CS	47.49	7.47	37.48	7.55
NN	56.74	6.43	32.92	3.91
NS	56.65	6.20	32.86	4.29

The concentration of O 1s over the catalyst SN could reach 46.85%, which illustrates that using FeSO<sub>4</sub> and Mg(NO<sub>3</sub>)<sub>2</sub> as precursors was in favor of the enrichment of oxygen on the surface of the catalyst and enhanced the surface oxidation ability.

Mg 1s and Ti 2p spectra of titanium modified FeMgO<sub>x</sub> catalysts with different precursors are shown in Figure 6. The Mg 1s peaks at a binding energy of about 1303 eV in, and coincides exactly with Mg<sup>2+</sup>. For the catalysts SN, SS, CN and CS, the Ti 2p<sub>3/2</sub> peaks at 458.23 eV and the Ti 2p<sub>1/2</sub> peaks at 464.03 eV were attributed to Ti<sup>4+</sup>. The binding energy of Ti 2p shifted higher compared with those of the catalysts NN and NS. The Ti 2p<sub>3/2</sub> peaks appeared at 458.23 eV and the Ti 2p<sub>1/2</sub> peaks appeared at 464.03 eV.

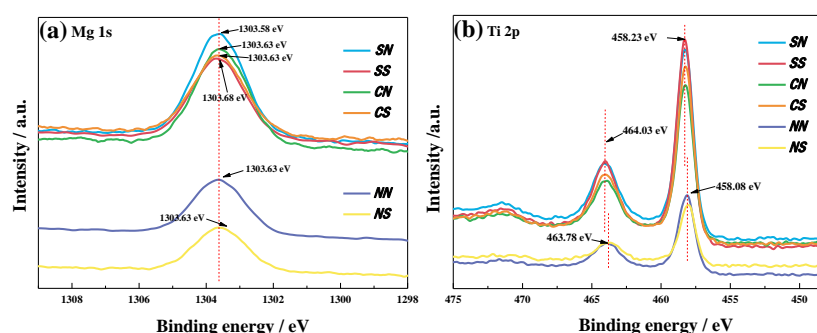


Figure 6. Mg 1s and Ti 2p spectra over titanium modified  $\text{FeMgO}_x$  catalysts with different precursors.

The Fe 2p spectra of titanium modified  $\text{FeMgO}_x$  catalysts with different precursors are shown in Figure 7. The Fe 2p spectra consisted of three overlapping peaks, and the binding energy of the Fe species were further analyzed by peak-fitting. The Fe  $2p_{3/2}$  peaks at binding energy around 710.0 eV and 712.0 eV, the Fe  $2p_{3/2,\text{sat}}$  peaks at binding energy about 718.8 eV and the Fe  $2p_{1/2}$  peaks at binding energy of 724.2 eV were all ascribed to  $\text{Fe}^{3+}$  [21].

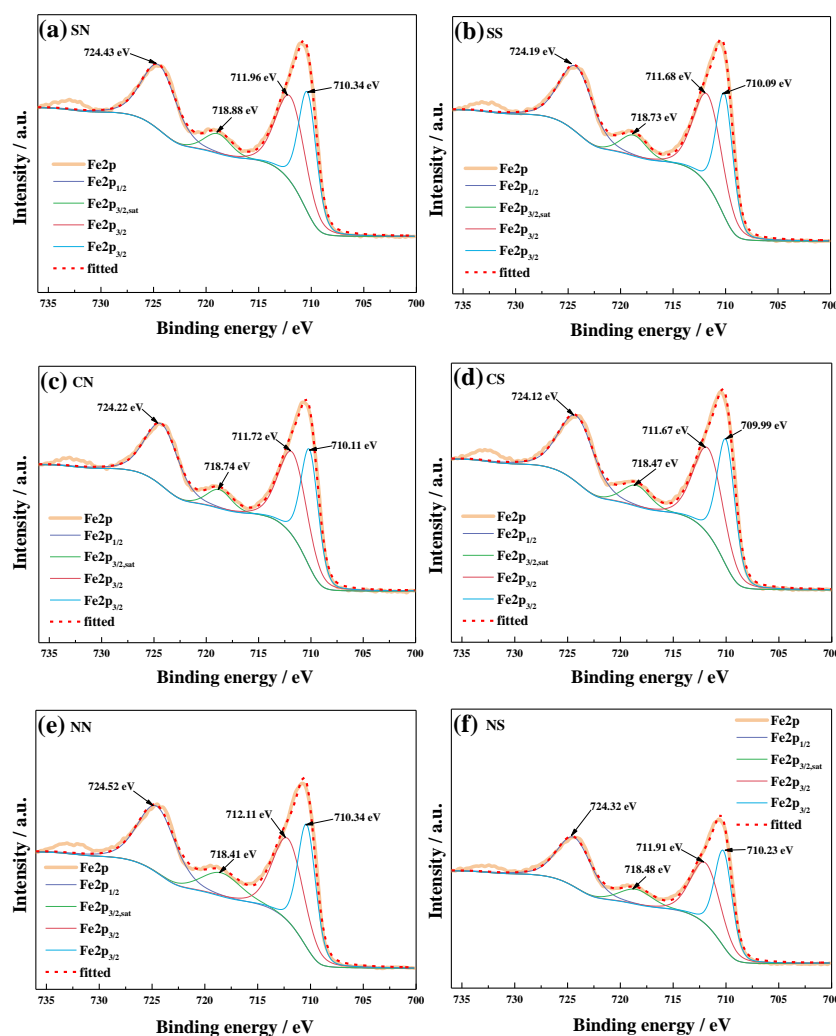
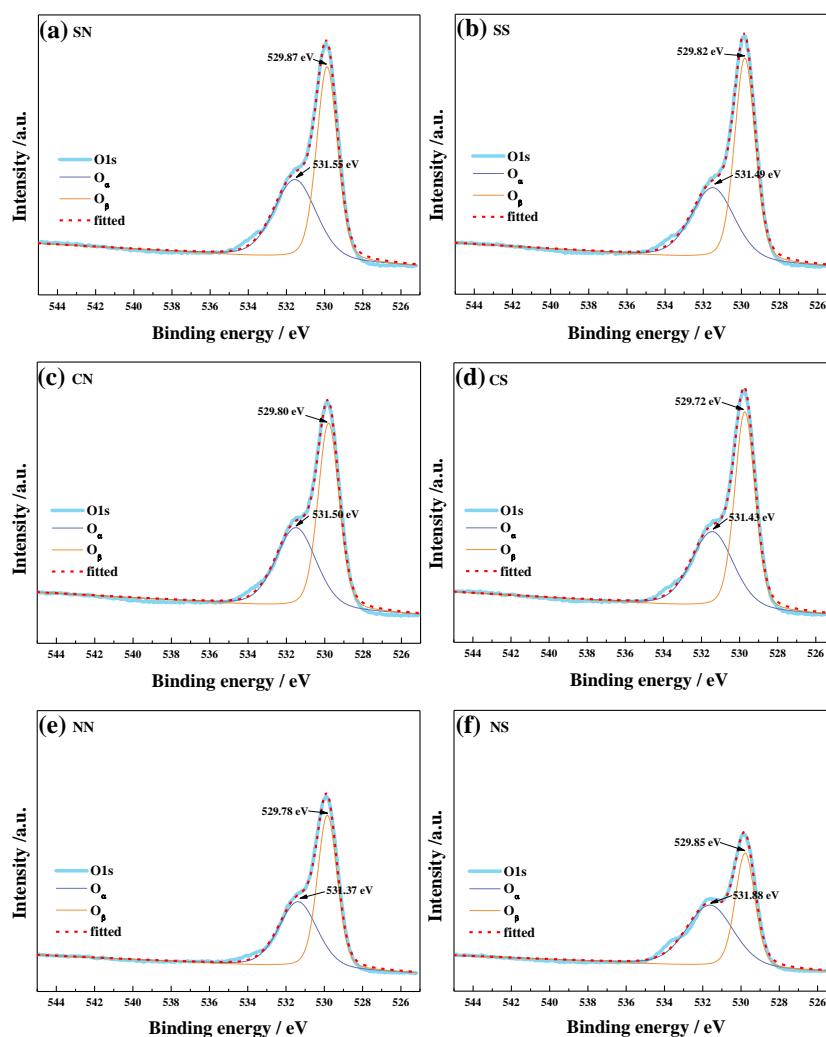


Figure 7. Fe 2p spectra of titanium modified  $\text{FeMgO}_x$  catalysts with different precursors.

The O 1s spectra of titanium modified  $\text{FeMgO}_x$  catalysts with different precursors are shown on Figure 8. The O 1s peaks at the binding energy of about 529.8 eV and 531.5 eV were the lattice oxygen

(denoted as  $O_{\beta}$ ) and the chemisorbed oxygen (denotes as  $O_{\alpha}$ ), respectively, which were both ascribed to  $O^{2-}$ . The intensity of the O 1s peaks of the catalysts NN and NS using  $Fe(NO_3)_3$  as precursor was apparently lower than those of the other catalysts, demonstrating that the concentration of oxygen on the surface of the catalysts NN and NS was low. Analyzed by peak-fitting, it could be seen that the chemisorbed oxygen, which was reported most active for the catalysts NN and NS, was significantly poorer, and the concentration of chemisorbed oxygen of the catalyst SN could be up to 21.2% on the surface, which was in accordance with the results above. Meanwhile, the shifting of the O 1s binding energy means that the oxygen deficit was on the surface of the catalyst, which was in favor of the SCR reaction.



**Figure 8.** O 1s spectra of titanium modified  $FeMgO_x$  catalysts with different precursors.

### 3.6. $NH_3$ -TPD

In the SCR reaction,  $NH_3$  should have firstly adsorbed and activated on the active sites and then reacted with NO, such as the Eley–Rideal mechanism, or reacted with both NO and adsorbed NO, such as the Langmuir–Hinshelwood mechanism. The presence of acid sites was of great importance for catalytic performance [45]. The surface acidity and acid species of titanium modified  $FeMgO_x$  catalysts were investigated by  $NH_3$ -TPD and the results are shown in Figure 9. Usually the  $NH_3$  desorption peaks below 300 °C were attributed to weak acid sites, and the  $NH_3$  desorption peaks above 300 °C were ascribed to strong acid sites. The  $NH_3$ -TPD profiles of all the catalysts exhibited a desorption peaks close to 170 °C, and the intensity of desorption peaks over the catalysts NN and

NS was apparently stronger than that of the catalysts SN, SS, CN and CS. The desorption peaks ascribe to strong acid sites of the catalysts SN, SS, CN and CS appeared at about 380 °C, while those of the catalysts NN and NS appeared above 450 °C. The amount of total acidity of all the catalysts was calculated as 1362.03  $\mu\text{mol/g}$ , 883.81  $\mu\text{mol/g}$ , 933.96  $\mu\text{mol/g}$ , 525.86  $\mu\text{mol/g}$ , 1915.58  $\mu\text{mol/g}$  and 1977.91  $\mu\text{mol/g}$ , with the order from catalyst SN to NS. Considering the activity results, it could be deduced that the weak acid sites that appeared at 170 °C had impact on the catalytic performance below 200 °C, and the strong acid sites that appeared at 380 °C made a great contribution to the catalytic activity and inhibited the secondary reaction at a higher temperature range. However, it was difficult for  $\text{NH}_3$  to absorb and activate on the strong acid site of the catalysts NN and NS, and appeared to exceed 450 °C. The total acidity of the catalyst SN reached 1362.03  $\mu\text{mol/g}$ , and the improvement of the total acidity of the catalyst SN could provide more adsorption sites. The enhancement of strong acid sites around 380 °C could inhibit the secondary reaction above 300 °C, which was the reason that the catalyst SN exhibited excellent catalytic performance and had a wide temperature range.

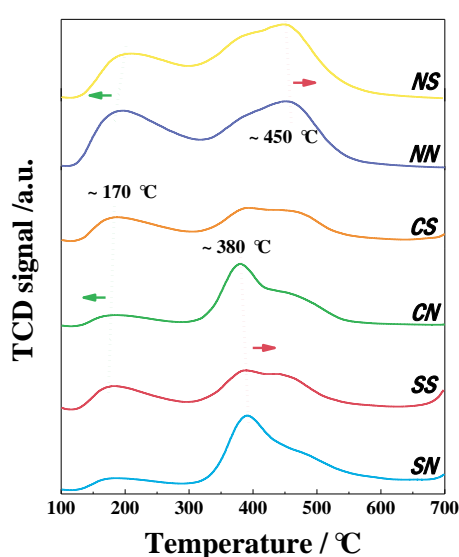


Figure 9.  $\text{NH}_3$ -TPD profiles over titanium modified  $\text{FeMgO}_x$  catalysts with different precursors.

#### 4. Conclusions

The influence of different precursors on titanium modified  $\text{FeMgO}_x$  catalysts was investigated and characterized. The results show that the crystalline phase of the active component was directly affected by the iron precursors.  $\gamma\text{-Fe}_2\text{O}_3$  formed as the main crystalline phase when  $\text{FeSO}_4$  and  $\text{FeCl}_2$  were used as precursors. The main crystalline phase would be amorphous iron-magnesium-titanium mixed oxides when  $\text{Fe}(\text{NO}_3)_3$  was used as precursor. The catalyst using  $\text{FeSO}_4$  and  $\text{Mg}(\text{NO}_3)_2$  as precursors exhibited  $\text{NO}_x$  conversion above 90% from 225 to 400 °C, while approaching 100% from 250 to 375 °C. The temperature window of the catalysts using  $\text{Fe}(\text{NO}_3)_3$  as a precursor shifted to lower temperature range, on which the secondary reaction occurred, leading to the decline of  $\text{NO}_x$  conversion at a high temperature. The regular spherical particle distribution and the good pores connectivity were advantageous to the mass transfer process. The acid sites that appeared at 170 °C played an important role for catalytic performance below 200 °C. The acid sites that appeared at 380 °C inhibited the secondary reaction at high temperature range. However, it was difficult for  $\text{NH}_3$  to absorb and activate on the strong acid sites using  $\text{Fe}(\text{NO}_3)_3$  as a precursor when exceeding 450 °C. The total acidity of the catalyst using  $\text{FeSO}_4$  and  $\text{Mg}(\text{NO}_3)_2$  as precursors could reach 1362.03  $\mu\text{mol/g}$ , and the surface oxygen concentration was also enhanced, thereby SCR reaction was improved correspondingly.

**Supplementary Materials:** The following are available online at <http://www.mdpi.com/2073-4344/9/6/560/s1>, Figure S1: Powder XRD patterns of Fe<sub>2</sub>O<sub>3</sub>.

**Author Contributions:** Conceptualization, D.W. and L.X.; methodology, D.W., Y.P. and L.X.; validation, J.L., Y.P. and D.W.; formal analysis, L.H. and Z.S.; investigation, L.X., Q.Y. and L.H.; resources, D.W. and C.L.; data curation, L.X. and Z.S.; writing—original draft preparation, L.X.; writing—review and editing, D.W.; visualization, L.X., L.H. and Z.S.; supervision, J.L. and C.L.; project administration, D.W., Y.P. and C.L.; funding acquisition, D.W., Y.P. and C.L.

**Funding:** This research was funded by the National Key Research and Development Program, grant number 2017YFC0212800 and 2017YFC0210200, the National Natural Science Foundation of China, grant number 21777081 and 51576117.

**Conflicts of Interest:** The authors declare no conflict of interest.

## References

1. Li, J.; Chang, H.; Ma, L.; Hao, J.; Yang, R.T. Low-temperature selective catalytic reduction of NO<sub>x</sub> with NH<sub>3</sub> over metal oxide and zeolite catalysts—A review. *Catal. Today* **2011**, *175*, 147–156. [[CrossRef](#)]
2. Baek, J.; Lee, S.; Park, J.; Jeong, J.; Hwang, R.; Ko, C.; Jeon, S.; Choi, T.; Yi, K. Effects of steam introduction on deactivation of Fe-BEA catalyst in NH<sub>3</sub>-SCR of N<sub>2</sub>O and NO. *J. Ind. Eng. Chem.* **2017**, *48*, 194–201. [[CrossRef](#)]
3. Boningari, T.; Smirniotis, P.G. Impact of nitrogen oxides on the environment and human health: Mn-based materials for the NO<sub>x</sub> abatement. *Curr. Opin. Chem. Eng.* **2016**, *13*, 133–141. [[CrossRef](#)]
4. Wang, D.; Luo, J.; Yang, Q.; Yan, J.; Zhang, K.; Zhang, W.; Peng, Y.; Li, J.; Crittenden, J. Deactivation mechanism of multipoisons in cement furnace flue gas on selective catalytic reduction catalysts. *Environ. Sci. Technol.* **2019**, *53*, 6937–6944. [[CrossRef](#)] [[PubMed](#)]
5. Skalska, K.; Miller, J.S.; Ledakowicz, S. Trends in NO<sub>x</sub> abatement: A review. *Sci. Total Environ.* **2010**, *408*, 3976–3989. [[CrossRef](#)]
6. Wang, D.; Chen, J.; Peng, Y.; Si, W.; Li, X.; Li, B.; Li, J. Dechlorination of chlorobenzene on vanadium-based catalysts for low-temperature SCR. *Chem. Commun.* **2018**, *54*, 2032–2035. [[CrossRef](#)] [[PubMed](#)]
7. Qi, G.; Yang, R.T. Performance and kinetics study for low-temperature SCR of NO with NH<sub>3</sub> over MnO<sub>x</sub>-CeO<sub>2</sub> catalyst. *J. Catal.* **2003**, *217*, 434–441. [[CrossRef](#)]
8. France, L.J.; Yang, Q.; Li, W.; Chen, Z.; Guang, J.; Guo, D.; Wang, L.; Li, X. Ceria modified FeMnO<sub>x</sub>—Enhanced performance and sulphur resistance for low-temperature SCR of NO<sub>x</sub>. *Appl. Catal. B Environ.* **2017**, *206*, 203–215. [[CrossRef](#)]
9. Shelef, M. Selective catalytic reduction of NO<sub>x</sub> with N-free reductants. *Chem. Rev.* **1995**, *95*, 209–225. [[CrossRef](#)]
10. Wang, D.; Peng, Y.; Yang, Q.; Xiong, S.; Li, J.; Crittenden, J. Performance of Modified La<sub>x</sub>Sr<sub>1-x</sub>MnO<sub>3</sub> Perovskite Catalysts for NH<sub>3</sub> Oxidation: TPD, DFT, and Kinetic Studies. *Environ. Sci. Technol.* **2018**, *52*, 7443–7449. [[CrossRef](#)]
11. Shi, X.; Liu, F.; Xie, L.; Shan, W.; He, H. NH<sub>3</sub>-SCR performance of fresh and hydrothermally aged Fe-ZSM-5 in standard and fast selective catalytic reduction reactions. *Environ. Sci. Technol.* **2013**, *47*, 3293–3298. [[CrossRef](#)] [[PubMed](#)]
12. Ko, J.; Park, R.; Jeon, J.; Kim, D.; Jung, S.; Kim, S.; Park, Y. Effect of surfactant, HCl and NH<sub>3</sub> treatments on the regeneration of waste activated carbon used in selective catalytic reduction unit. *J. Ind. Eng. Chem.* **2015**, *32*, 109–112. [[CrossRef](#)]
13. Fan, Y.; Ling, W.; Huang, B.; Dong, L.; Yu, C.; Xi, H. The synergistic effects of cerium presence in the framework and the surface resistance to SO<sub>2</sub> and H<sub>2</sub>O in NH<sub>3</sub>-SCR. *J. Ind. Eng. Chem.* **2017**, *56*, 108–119. [[CrossRef](#)]
14. Boningari, T.; Ettireddy, P.R.; Somogyvari, A.; Liu, Y.; Vorontsov, A.; McDonald, C.A.; Smirniotis, P.G. Influence of elevated surface texture hydrated titania on Ce-doped Mn/TiO<sub>2</sub> catalysts for the low-temperature SCR of NO<sub>x</sub> under oxygen-rich conditions. *J. Catal.* **2016**, *325*, 145–155. [[CrossRef](#)]
15. Aguilar-Romero, M.; Camposeco, R.; Castillo, S.; Marín, J.; Rodríguez-González, V.; García-Serrano, L.; Mejía-Centeno, I. Acidity, surface species, and catalytic activity study on V<sub>2</sub>O<sub>5</sub>-WO<sub>3</sub>/TiO<sub>2</sub> nanotube catalysts for selective NO reduction by NH<sub>3</sub>. *Fuel* **2017**, *198*, 123–133. [[CrossRef](#)]
16. Pappas, D.K.; Boningari, T.; Boolchand, P.; Smirniotis, P.G. Novel manganese oxide confined interweaved titania nanotubes for the low-temperature Selective Catalytic Reduction (SCR) of NO<sub>x</sub> by NH<sub>3</sub>. *J. Catal.* **2016**, *334*, 1–13. [[CrossRef](#)]

17. Song, I.; Youn, S.; Lee, H.; Lee, S.G.; Cho, S.; Kim, D. Effects of microporous TiO<sub>2</sub> support on the catalytic and structural properties of V<sub>2</sub>O<sub>5</sub>/microporous TiO<sub>2</sub> for the selective catalytic reduction of NO by NH<sub>3</sub>. *Appl. Catal. B Environ.* **2017**, *210*, 421–431. [[CrossRef](#)]
18. Thirupathi, B.; Smirniotis, P.G. Nickel-doped Mn/TiO<sub>2</sub> as an efficient catalyst for the low-temperature SCR of NO with NH<sub>3</sub>: Catalytic evaluation and characterizations. *J. Catal.* **2012**, *288*, 74–83. [[CrossRef](#)]
19. He, Y.; Ford, M.E.; Zhu, M.; Liu, Q.; Tumuluri, U.; Wu, Z.; Wachs, I.E. Influence of catalyst synthesis method on selective catalytic reduction (SCR) of NO by NH<sub>3</sub> with V<sub>2</sub>O<sub>5</sub>-WO<sub>3</sub>/TiO<sub>2</sub> catalysts. *Appl. Catal. B* **2016**, *193*, 141–150. [[CrossRef](#)]
20. Xu, H.; Li, Y.; Xu, B.; Cao, Y.; Feng, X.; Sun, M.; Gong, M.; Chen, Y. Effectively promote catalytic performance by adjusting W/Fe molar ratio of FeW<sub>x</sub>/CeO<sub>2</sub>. 68ZrO<sub>2</sub> monolithic catalyst for NH<sub>3</sub>-SCR. *J. Ind. Eng. Chem.* **2016**, *36*, 334–345. [[CrossRef](#)]
21. Wang, D.; Peng, Y.; Xiong, S.; Li, B.; Gan, L.; Lu, C.; Chen, J.; Ma, Y.; Li, J. De-reducibility mechanism of titanium on maghemite catalysts for the SCR reaction: An in situ DRIFTS and quantitative kinetics study. *Appl. Catal. B* **2018**, *221*, 556–564. [[CrossRef](#)]
22. Liu, F.; He, H.; Zhang, C.; Feng, Z.; Zheng, L.; Xie, Y.; Hu, T. Selective catalytic reduction of NO with NH<sub>3</sub> over iron titanate catalyst: Catalytic performance and characterization. *Appl. Catal. B Environ.* **2010**, *96*, 408–420. [[CrossRef](#)]
23. Yang, S.; Li, J.; Wang, C.; Chen, J.; Ma, L.; Chang, H.; Chen, L.; Peng, Y.; Yan, N. Fe–Ti spinel for the selective catalytic reduction of NO with NH<sub>3</sub>: Mechanism and structure–activity relationship. *Appl. Catal. B Environ.* **2012**, *117*, 73–80. [[CrossRef](#)]
24. Liu, Z.; Liu, Y.; Chen, B.; Zhu, T.; Ma, L. Novel Fe–Ce–Ti catalyst with remarkable performance for the selective catalytic reduction of NO<sub>x</sub> by NH<sub>3</sub>. *Catal. Sci. Technol.* **2016**, *6*, 6688–6696. [[CrossRef](#)]
25. Du, X.; Wang, X.; Chen, Y.; Gao, X.; Zhang, L. Supported metal sulfates on Ce–TiO<sub>x</sub> as catalysts for NH<sub>3</sub>-SCR of NO: High resistances to SO<sub>2</sub> and potassium. *J. Ind. Eng. Chem.* **2016**, *36*, 271–278. [[CrossRef](#)]
26. Xiong, Z.; Peng, B.; Zhou, F.; Wu, C.; Lu, W.; Jin, J.; Ding, S. Magnetic iron-cerium-tungsten mixed oxide pellets prepared through critic acid sol-gel process assisted by microwave irradiation for selective catalytic reduction of NO<sub>x</sub> with NH<sub>3</sub>. *Powder Technol.* **2017**, *319*, 19–25. [[CrossRef](#)]
27. Xiong, Z.; Liu, J.; Zhou, F.; Liu, D.; Lu, W.; Jin, J.; Ding, S. Selective catalytic reduction of NO<sub>x</sub> with NH<sub>3</sub> over iron-cerium-tungsten mixed oxide catalyst prepared by different methods. *Appl. Surf. Sci.* **2017**, *406*, 218–225. [[CrossRef](#)]
28. Xu, H.; Xie, J.; Ma, Y.; Qu, Z.; Zhao, S.; Chen, W.; Huang, W.; Yan, N. The cooperation of FeSn in a MnO<sub>x</sub> complex sorbent used for capturing elemental mercury. *Fuel* **2015**, *140*, 803–809. [[CrossRef](#)]
29. Shu, Y.; Aikebaier, T.; Quan, X.; Chen, S.; Yu, H. Selective catalytic reaction of NO<sub>x</sub> with NH<sub>3</sub> over Ce–Fe/TiO<sub>2</sub>-loaded wire-mesh honeycomb: Resistance to SO<sub>2</sub> poisoning. *Appl. Catal. B Environ.* **2014**, *150*, 630–635. [[CrossRef](#)]
30. Liu, Z.; Su, H.; Chen, B.; Li, J.; Woo, S. Activity enhancement of WO<sub>3</sub> modified Fe<sub>2</sub>O<sub>3</sub> catalyst for the selective catalytic reduction of NO<sub>x</sub> by NH<sub>3</sub>. *Chem. Eng. J.* **2016**, *299*, 255–262. [[CrossRef](#)]
31. Foo, R.; Vazhnova, T.; Lukyanov, D.B.; Millington, P.; Collier, J.; Rajaram, R.; Golunski, S. Formation of reactive Lewis acid sites on Fe/WO<sub>3</sub>-ZrO<sub>2</sub> catalysts for higher temperature SCR applications. *Appl. Catal. B Environ.* **2015**, *162*, 174–179. [[CrossRef](#)]
32. Putluru, S.S.R.; Schill, L.; Jensen, A.D.; Siret, B.; Tabaries, F.; Fehrmann, R. Mn/TiO<sub>2</sub> and Mn–Fe/TiO<sub>2</sub> catalysts synthesized by deposition precipitation—Promising for selective catalytic reduction of NO with NH<sub>3</sub> at low temperatures. *Appl. Catal. B Environ.* **2015**, *165*, 628–635. [[CrossRef](#)]
33. Wu, S.; Zhang, L.; Wang, X.; Zou, W.; Cao, Y.; Sun, J.; Tang, C.; Gao, F.; Deng, Y.; Dong, L. Synthesis, characterization and catalytic performance of FeMnTiO<sub>x</sub> mixed oxides catalyst prepared by a CTAB-assisted process for mid-low temperature NH<sub>3</sub>-SCR. *Appl. Catal. A Gen.* **2015**, *505*, 235–242. [[CrossRef](#)]
34. Qi, G.; Yang, R.T.; Chang, R. MnO<sub>x</sub>-CeO<sub>2</sub> mixed oxides prepared by co-precipitation for selective catalytic reduction of NO with NH<sub>3</sub> at low temperatures. *Appl. Catal. B Environ.* **2004**, *51*, 93–106. [[CrossRef](#)]
35. Xiong, Z.; Wu, C.; Hu, Q.; Wang, Y.; Jin, J.; Lu, C.; Guo, D. Promotional effect of microwave hydrothermal treatment on the low-temperature NH<sub>3</sub>-SCR activity over iron-based catalyst. *Chem. Eng. J.* **2016**, *286*, 459–466. [[CrossRef](#)]

36. Cao, F.; Su, S.; Xiang, J.; Wang, P.; Hu, S.; Sun, L.; Zhang, A. The activity and mechanism study of Fe–Mn–Ce/ $\gamma$ -Al<sub>2</sub>O<sub>3</sub> catalyst for low temperature selective catalytic reduction of NO with NH<sub>3</sub>. *Fuel* **2015**, *139*, 232–239. [[CrossRef](#)]
37. Casanova, M.; Llorca, J.; Sagar, A.; Schermanz, K.; Trovarelli, A. Mixed iron–erbium vanadate NH<sub>3</sub>-SCR catalysts. *Catal. Today* **2015**, *241*, 159–168. [[CrossRef](#)]
38. Zhu, L.; Zhong, Z.; Yang, H.; Wang, C. Comparison study of Cu-Fe-Ti and Co-Fe-Ti oxide catalysts for selective catalytic reduction of NO with NH<sub>3</sub> at low temperature. *J. Colloid Interface Sci.* **2016**, *478*, 11–21. [[CrossRef](#)]
39. Liu, F.; He, H.; Zhang, C.; Shan, W.; Shi, X. Mechanism of the selective catalytic reduction of NO<sub>x</sub> with NH<sub>3</sub> over environmental-friendly iron titanate catalyst. *Catal. Today* **2011**, *175*, 18–25. [[CrossRef](#)]
40. Liu, F.; He, H. Structure–Activity Relationship of Iron Titanate Catalysts in the Selective Catalytic Reduction of NO<sub>x</sub> with NH<sub>3</sub>. *J. Phys. Chem. C* **2010**, *114*, 16929–16936. [[CrossRef](#)]
41. Ma, L.; Li, J.; Ke, R.; Fu, L. Catalytic Performance, Characterization, and Mechanism Study of Fe<sub>2</sub>(SO<sub>4</sub>)<sub>3</sub>/TiO<sub>2</sub> Catalyst for Selective Catalytic Reduction of NO<sub>x</sub> by Ammonia. *J. Phys. Chem. C* **2011**, *115*, 7603–7612. [[CrossRef](#)]
42. Xu, L.; Niu, S.; Lu, C.; Wang, D.; Zhang, K.; Li, J. NH<sub>3</sub>-SCR performance and characterization over magnetic iron-magnesium mixed oxide catalysts. *Korean J. Chem. Eng.* **2017**, *34*, 1576–1583. [[CrossRef](#)]
43. Xu, L.; Niu, S.; Wang, D.; Lu, C.; Zhang, Q.; Zhang, K.; Li, J. Selective catalytic reduction of NO<sub>x</sub> with NH<sub>3</sub> over titanium modified Fe<sub>x</sub>Mg<sub>y</sub>O<sub>z</sub> catalysts: Performance and characterization. *J. Ind. Eng. Chem.* **2018**, *63*, 391–404. [[CrossRef](#)]
44. Xu, L.; Niu, S.; Lu, C.; Zhang, Q.; Li, J. Influence of calcination temperature on Fe<sub>0.8</sub>Mg<sub>0.2</sub>O<sub>z</sub> catalyst for selective catalytic reduction of NO<sub>x</sub> with NH<sub>3</sub>. *Fuel* **2018**, *219*, 248–258. [[CrossRef](#)]
45. Wang, D.; Peng, Y.; Yang, Q.; Hu, F.; Li, J.; Crittenden, J. NH<sub>3</sub>-SCR performance of WO<sub>3</sub> blanketed CeO<sub>2</sub> with different morphology: Balance of surface reducibility and acidity. *Catal. Today* **2019**, *332*, 42–48. [[CrossRef](#)]



© 2019 by the authors. Licensee MDPI, Basel, Switzerland. This article is an open access article distributed under the terms and conditions of the Creative Commons Attribution (CC BY) license (<http://creativecommons.org/licenses/by/4.0/>).